ACS APPLIED MATERIALS & INTERFACES

www.acsami.org

Research Article

# Exceptional Viscoelastic Properties in Graphene Oxide Films

Gehan C. Jayatilaka, Athena Aber, Moein Mohammadi, Vahid Morovati, and Mehran Tehrani*

Cite This: *ACS Appl. Mater. Interfaces* 2024, 16, 11778−11786

Read Online

ACCESS | Metrics & More | Article Recommendations | Supporting Information

**ABSTRACT:** Materials that combine high stiffness with effective damping are in high demand across various industries. While polymers excel in damping, they often lack stiffness and thermal stability. Conversely, metals and ceramics boast high mechanical and thermal properties but lack damping. This study demonstrates that graphene oxide (GO) and reduced graphene oxide (rGO) films can achieve exceptional viscoelastic properties across a wide temperature range. Furthermore, it explains the damping mechanisms and structural characteristics that influence the unique viscoelastic behavior of GO and rGO films. Through comprehensive characterizations, this study correlates the structure and spatial variation in local strain (measured with in situ Raman microscopy) of GO and rGO films with their storage and loss moduli. This correlation links these properties to the water loss as a function of the temperature rise. GO and rGO films exhibited a damping coefficient of 0.2−0.4 while maintaining stiffness values of 10−20 GPa in the 30−120 °C range. These high damping values were attributed to intermittent slippage and hydrogen bond density between the constituent sheets. Numerical modeling was conducted to further elucidate the mechanisms responsible for the properties noted in these films. This study enhances our understanding of the viscoelastic properties of GO films and offers a new potential material for applications across various fields.

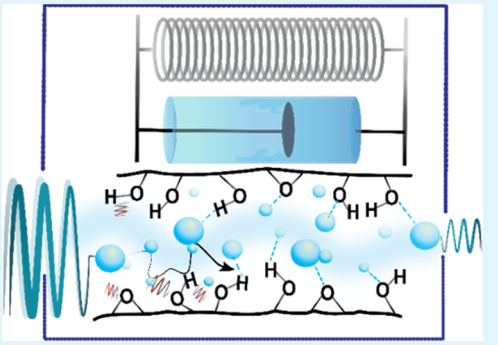

**KEYWORDS:** *damping, graphene oxide, viscoelastic properties, dynamic mechanical analysis, modeling*



## 1. INTRODUCTION

High damping materials are essential in engineering design, especially in civilian and military machinery, to reduce mechanical vibrations, resist impact damage, and attenuate wave propagation. For example, mechanical vibrations can have detrimental effects on structural components, reducing their fatigue life. For high damping materials to be used practically, they must also possess adequate mechanical properties[1,2] and service temperature range.[3] Damping materials used in the industry can perform well under specific conditions of temperature, amplitude, and frequency; however, a material that exhibits high damping over a broad range of conditions while also demonstrating robust thermo-mechanical performance would be beneficial for a diverse range of applications.[4]

Most traditional damping materials can be classified into two categories: (1) polymers and (2) metal matrix composites. There are reports of exceptional viscoelastic materials, including ceramic aerogels[5] and metal alloys.[6] However, their feasibility for use in structural applications is constrained. Polymeric materials achieve exceptional damping in a narrow temperature region close to their glass transition temperature.[3] Most of these polymer-based dampers, like rubber, exhibit low stiffnesses.[7] Metals, on the other hand, exhibit high stiffness and thermal stability but have poor damping if not reinforced.[1,8] Reinforcing metals with fillers to enhance their damping has proven to be both costly and challenging.[7] These limitations have imposed design constraints on structural design practices in the industry. Damping materials and structures are often added to structural components to attenuate vibrations; however, they operate only within certain temperature and strain (stress) ranges. Nanomaterials provide a method to circumvent these limitations.

Nanomaterials provide extensive surface areas for utilization and the opportunity for the construction of multiscale structures, resulting in tailored viscoelastic properties. For instance, one study found that adding carbon nanotubes as fillers in a polymer matrix can increase the damping properties through friction caused by stick−slip motion between filler and resin.[9] Graphene nanoplatelets also have been found to possess high damping capabilities, due to their corrugated-like structure that facilitate high energy dispersion.[10] Graphene oxide (GO) is another nanomaterial that has garnered significant attention due to its outstanding thermo-mechanical properties, affordability, and water processability.

Graphene oxide has previously been used as a composite additive in polymer and ceramic composites to increase their

Received: October 19, 2023
Revised: February 6, 2024
Accepted: February 7, 2024
Published: February 26, 2024

damping.[11−13] Graphene oxide, a modified form of graphene, is composed of graphene sheets predominantly functionalized with carboxyl, hydroxyl, or epoxide groups.[14] Free-standing films can be made easily via several approaches, e.g., vacuum filtration of graphene oxide dispersed in water. These films are composed of several well-ordered multilayer graphene particles or nanosheets, achieving high stiffness and strength at a low density.[15] Reduction of graphene oxide, creating reduced graphene oxide (rGO), can bring the material closer to the pristine properties of graphene through the removal of oxygen-containing functional groups.[16]

This work examines the viscoelastic properties of GO and rGO films as high damping materials offering substantial stiffness and a broad service temperature range. The viscoelastic properties of these materials could potentially be generated by a combination of several mechanisms at the nano and micron scales. One of these mechanisms involves the presence of hydrogen bonds and intercalated water between the GO layers. GO films are composed of particles linked together by mainly hydrogen bonds via oxygen-containing functional groups. When under stress, hydrogen bonds between layers break and reform as layers slide; this continuous breakage of bonds is possibly a major source of energy dissipation.[17] GO is hydrophilic, which causes GO particles to bond both directly to each other and indirectly through water molecules. rGO, on the other hand, is partially hydrophobic and shows a different viscoelastic response as a result.[18] Moisture content has been shown to affect the hydrogen bonding between GO platelets.[19] Intercalated water can lead to many interesting viscoelastic properties not commonly seen in other materials. Another possible mechanism for energy dissipation is crack bridging. Crack bridging, typically seen in ceramic and composite materials, occurs when elongated grains or fillers continue to carry a load in the wake of a propagating crack. These bridges shield the crack tip from global stresses, increasing the toughness of the material before catastrophic crack propagation. These bridges can also increase the friction between cracks.[20] This is a potential source of damping in the GO and rGO films studied here.

In addition to these mechanisms, there are certain structural and stress-related aspects believed to affect the viscoelastic properties of this material, such as the rearrangement of layers during loading and the corrugation of GO and rGO layers. Rearrangement occurs when weakly bound GO sheets slide into a configuration that is strongly bound, increasing the overall stiffness.[15] Due to the low bending stiffness of GO sheets, layers are full of corrugations or waves.[21] These layers rubbing together can lead to high energy dissipation, in which energy is dispersed through friction; a possible origin of high damping in GO.[22] This waviness pattern has a significant effect on the deformation behavior of GO films. Models of the interaction of corrugated GO particles show how the wrinkled nature of GO films can lead to a significant drop in stiffness.[23] GO sheets that are more functionalized show a higher degree of wrinkles, which can lead to different viscoelastic responses.[23,24]

While the mechanical properties of graphene oxide have been thoroughly investigated, their damping behavior has received relatively little attention. A few studies have investigated the viscoelasticity of GO films;[25−28] however, there is still a knowledge gap regarding how GO films achieve both high damping and stiffness simultaneously. This study aims to provide deeper insights into the mechanisms that generate the unique viscoelastic properties of GO and rGO films as well as into the structural aspects that influence them. In particular, it investigates the effects of temperature and water content on interparticle bonds and the overall viscoelastic properties of GO and rGO films. These findings are then correlated with spatial variation of stress, as observed through in situ tensile Raman mapping, water content, interlayer spacing between sheets, and their structure, as seen via electron microscopy. These correlations reveal the mechanisms that control the viscoelastic behavior of the GO and rGO films. A mechanics-based model is also proposed and utilized to relate the structural changes due to temperature change and water intercalation content to damping and stiffness values measured experimentally. The exceptional damping properties of the films reported in this study, along with their remarkable mechanical and thermal properties, render them multifunctional materials with vast potential for various applications.

## 2. METHODS

**2.1. Experimental Section.** Graphene oxide dispersed in water (4 mg/mL) was purchased from Sigma-Aldrich (777676). The 57% hydroiodic acid (HI) solution used for GO reduction was purchased from Sigma-Aldrich (210021) and used as received. Graphene oxide films were fabricated via vacuum filtration. The GO solution was diluted with deionized water to a concentration of 0.5 mg/mL. The diluted solution was then sonicated in a Cole-Parmer Ultrasonic Cleaner at a frequency of 40 kHz for 15 min to produce a homogeneous solution. The films were then prepared by filtration on an MF-Millipore cellulose membrane with a pore size of 0.22 $\mu$m. The produced films had a diameter of 37.5 mm and a thickness of approximately 10 $\mu$m (measured using SEM). For testing and characterization, these films are cut into rectangular film strips with a width of 3 mm and a length of 20 mm. Reduced graphene oxide specimens were prepared by chemical reduction using a 57% HI solution. The graphene oxide film strips were submerged in HI solution for 1 h at room temperature. To remove excess HI solution, the film strips were washed by being submerged alternately in an ethanol bath and then in a deionized water solution bath five times. After the chemical reduction process, these rGO film strips achieved a thickness of approximately 7 $\mu$m. The reduction of GO is confirmed in the Fourier transform infrared (FTIR) spectroscopy and X-ray photoelectron spectroscopy (XPS) results in Figures S1 and S2, respectively, in the Supporting Information.

A common way to quantify the damping, or absorption and dispersion of mechanical energy, is to observe the tan $\delta$ (quantification of the dispersion of energy) of a material under cyclic loading by using dynamic mechanical analysis (DMA). All DMA tests were carried out using a Netzsch DMA 242 E Artemis. All film strips were tested in tension mode with a gauge length of 15 mm. These tests were force-constant amplitude-fixed and set to 0.1% strain. GO samples were oscillated at a fixed frequency of 1 Hz, unless stated otherwise, between 35 and 90 °C, while rGO samples were oscillated at the same fixed frequency from 35 to 120 °C; furnace temperature was ramped up at 2.5 °C/min. The storage modulus represents the elastic response (on a macroscale), while the loss modulus represents the viscous response or energy dissipated per unit volume per unit deformation. Tan $\delta$ is usually used to quantify the ability to dissipate energy or damping in a material.

A Mettler Thermogravimetric Analyzer Model TGA/DSC 1 was used for the TGA testing. Film strips of both GO and rGO were placed in an alumina crucible for testing. The tests were run in air. For the GO film sample, the temperature was ramped from room temperature to 90 °C and back twice over, then once more to 140 °C and back. The rGO sample followed the same process except the maximum temperature of the first two cycles was 120 °C rather than


https://doi.org/10.1021/acsami.3c15671
ACS Appl. Mater. Interfaces 2024, 16, 11778−11786

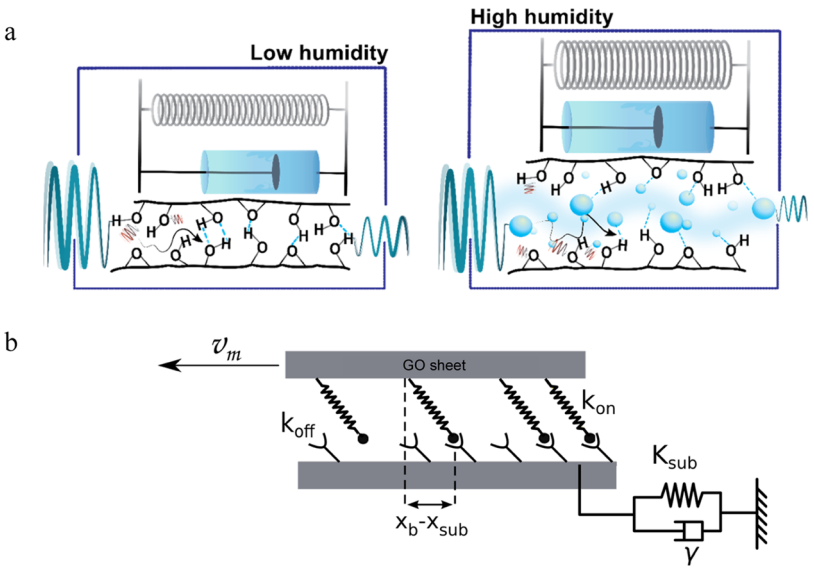


**Figure 1.** (a) Schematic of how intercalated water affects bonding between GO sheets. (b) Diagram representation of the formation and disassociation of hydrogen bonds due to in-plane shear deformation applied to GO.

90 °C. Both samples were heated at a rate of 2.5 °C/min to match the heating rate (and water loss) in the DMA tests. The cooling rates in these TGA tests were also at a rate of 2.5 °C/min.

Raman maps were obtained by using a Witec Raman Spectrometer at an excitation wavelength of 532 nm. The laser was focused on the top surface of each film sample. A total number of 10 accumulations with an integration time of 4 s was used to collect the single spectra for GO and rGO samples. For in situ Raman mapping, the samples were placed in tension in a Linkam Modular Force Stage, and maps were taken at various strain values. Maps were made with 100 spectra points in a 150 $\mu$m × 150 $\mu$m area. Each spectra point was a single accumulation with an integration time of 10 s.

XRD measurements of the film strips before and after DMA testing were carried out in a Rigaku Miniflex 600 Diffractometer. The voltage and current used for these measurements were 40 kV and 15 mA, respectively. The film strips were placed on a glass substrate and measured from 5 to 60° ($\theta$) at a rate of 2.5 degrees/min. The fwhm and peak center were measured by using a nonlinear Gauss curve fit.

SEM was used to measure the particle size of individual GO particles. For sample preparation, around 10 $\mu$L of GO dispersed in water (0.1 mg/mL) was drop-cast onto a glass substrate, and the water was rapidly evaporated using a heating plate. ImageJ software was utilized to measure individual particle sizes in the SEM micrographs. Cross-sectional SEM imaging was also used to assess the layered structure of the fabricated films.

**2.2. Modeling.** The interaction between layers in a GO film is examined using a simplified numerical model that captures only captures particle−particle interactions. Parallel planes connected via multiple mass-spring dampers represent GO layers bonded by hydrogen bonds. The current understanding of stress transfer in this study relies on dynamic disassociation mechanisms, which account for the force transmission between graphene oxide sheets through active hydrogen bonds. It is suggested that the breakage of these dynamic bonds enables GO sheets to slide at low loading rates. Additionally, the rebonding of broken bonds contributes to a self-healing-like behavior, significantly contributing to the energy dissipation observed in GO films. The bonding and subsequent breakage are responsible for the complex dynamic behavior exhibited in the DMA response of the GO films. A schematic of how these water molecules interact with graphene oxide is shown in Figure 1a.

Figure 1b depicts a simplified representation, where two parallel GO plates are interconnected by dynamic bonds. The bottom plate remains stationary, while the other plate moves at a constant velocity. The relative displacement between plates induces a shear force within the dynamic bonds, potentially leading to bond breakages. The broken bonds then move to adjacent bonding sites and form new bonds. It is assumed that these bonds do not retain their bonding history and that each free bonding site has the potential to form new bonds. Thus, the macroscopic behavior of a material with a large number of bonds can be described by observing the combined behavior of individual bonds. Here, the analysis begins by examining the mechanics of the bonds between two sheets and subsequently extends the findings to understand the macroscopic behavior of GO films. The average response of the individual bonds primarily informs the overall behavior of the films.

The model is composed of two key components: free functional groups and graphene oxide layers acting as the dynamic bonds' substrate. The layers are interconnected by a certain number of active hydrogen bonds ($N_a$), which can undergo breakage and rebonding with the free connectors to form new bonds. In this context, it is assumed that the connectors can exist in either free or bonded states. To capture the behavior of the hydrogen bonds under shear deformation, these bonds are modeled as Hookean springs with stiffness parameter $K_b$. It is assumed that hydrogen bonds exhibit linear behavior for simplicity.[29] Additionally, it is assumed that the stiffness of the GO layers is significantly higher than that of the hydrogen bonds. Consequently, the force transferred between the layers is approximated as $f_b = K_b(x_b - x_{sub})$, where $x_b$ and $x_{sub}$ represent the displacements of each end of the hydrogen bond.

Assuming the total number of connectors is conserved during loading history, one can calculate their total number as $N_{tot} = \int_A (\rho_a + \rho_d)dA$, where $\rho_a$ and $\rho_d$ are the densities of active and deactivated bonds per unit of area, respectively. By considering a coupled first-order kinetic bond disassociation/reassociation model, the total number of active bonds as a function of deformation history can be calculated as

$$\frac{d\rho_a}{dt} = -k_{off}\rho_a + k_{on}\rho_d$$
$$\frac{d\rho_d}{dt} = k_{off}\rho_a - k_{on}\rho_d \quad (1)$$

where $k_{on}(T)$ and $k_{off}(f)$ are the association and dissociation rates dependent on temperature and force, respectively. The association rate is assumed to be a linear function of the bond force as $k_{off} = k_{off}^0 + \alpha_{off}f$. Thus, as the rate of deformation increases, the association rate also increases, resulting in a higher dissipation between the GO sheets. The association rate is modeled using the Arrhenius function to consider the temperature dependency of the reformation of bonds.


https://doi.org/10.1021/acsami.3c15671
ACS Appl. Mater. Interfaces 2024, 16, 11778−11786

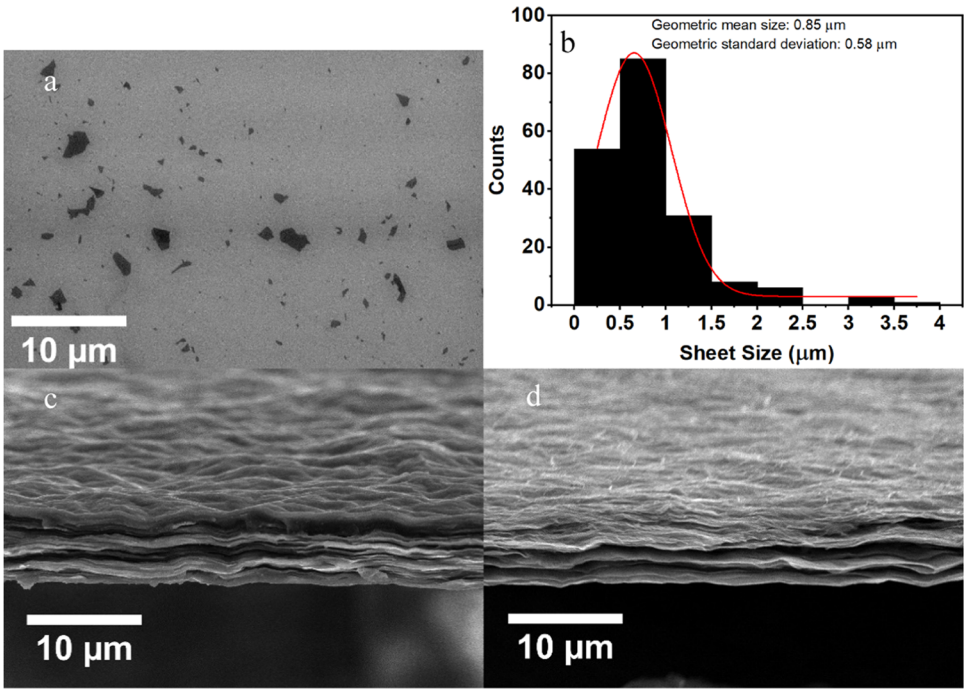


**Figure 2.** (a) SEM image of individual GO particles and (b) GO particle size histogram. Micrographs of the tensile fractured cross sections of (c) GO and (d) rGO films.

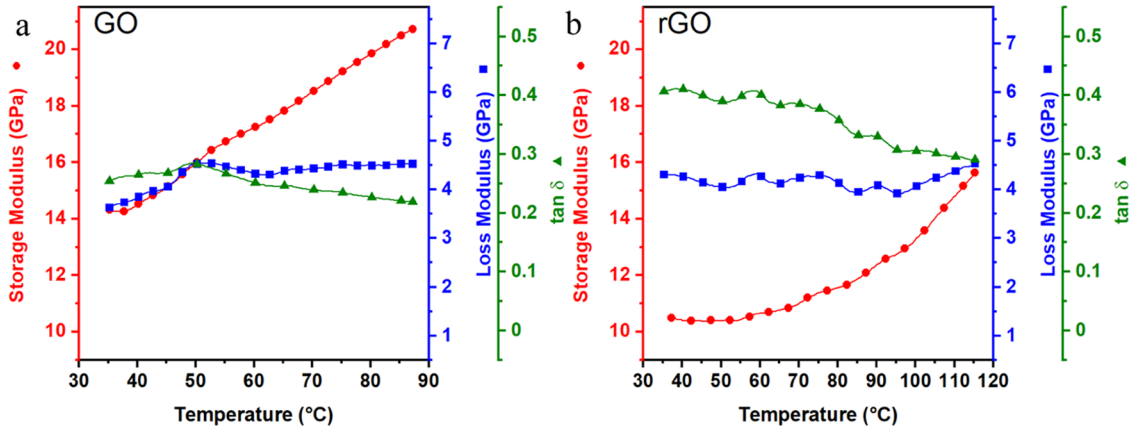


**Figure 3.** DMA results of the storage modulus, loss modulus, and tan $\delta$ for (a) GO and (b) rGO film strip samples with respect to temperature.

In addition, the GO sheets are assumed to be connected through the viscoelastic Kelvin–Voigt model to consider the effects of multilayer GO sheets sliding on top of each other and the presence of water between the layers. Thus, the equation of motion for viscoelastic GO particles is derived considering the force equilibrium applied on the sheets as

$$\gamma\dot{x} + k_{sub}x_{sub} = n_a K_b(x - x_{sub}) \tag{2}$$

Equations 1 and 2 are solved simultaneously using the finite-difference method to investigate the dynamics of the hydrogen bonds in the graphene oxide papers. To extrapolate the behavior of the bulk films using the theory described in the manuscript, a continuum model was employed to capture the macroscale behavior of the graphene oxide (GO) film under cyclic deformation. The energy stored in bonds is dependent on bond length and relative deformation between GO sheets, denoted as $\psi_b = \phi(|x - x_b|)$. Dissipation occurs when a bond breaks, and it is assumed that the energy stored in the bond is instantaneously released. The dissipated energy is released into the environment in the form of heat, and its impact on future bonding is assumed to be negligible.

The macroscopic response of the material is estimated by calculating the average behavior of bonds at each time instant. The total energy of the system can be calculated by summing the forces in dynamic bonds and considering the behavior of the GO sheets. Additionally, the evolution of the number of bonds is assumed to follow a fractional function.

$$\frac{d}{dt}(N_a) = -\frac{1}{t_R}(N_a)^{\alpha} \rightarrow N_a(t, \tau) = N_{a0}(T)\left(1 + \frac{(\alpha - 1)(t - \tau)}{t_B}\right)^{1/1-\alpha} \tag{3}$$

where it assumed that the initial number of bonds ($N_{a0}(T)$) increases due to a change in distance between sheets as temperature increases using an Arrhenius relation. The conducted experiments illustrate a direct correlation between temperature increase and reduction of intersheet distance of GO sheets. The bond reattachment rate is determined by[30]


https://doi.org/10.1021/acsami.3c15671
ACS Appl. Mater. Interfaces 2024, 16, 11778−11786

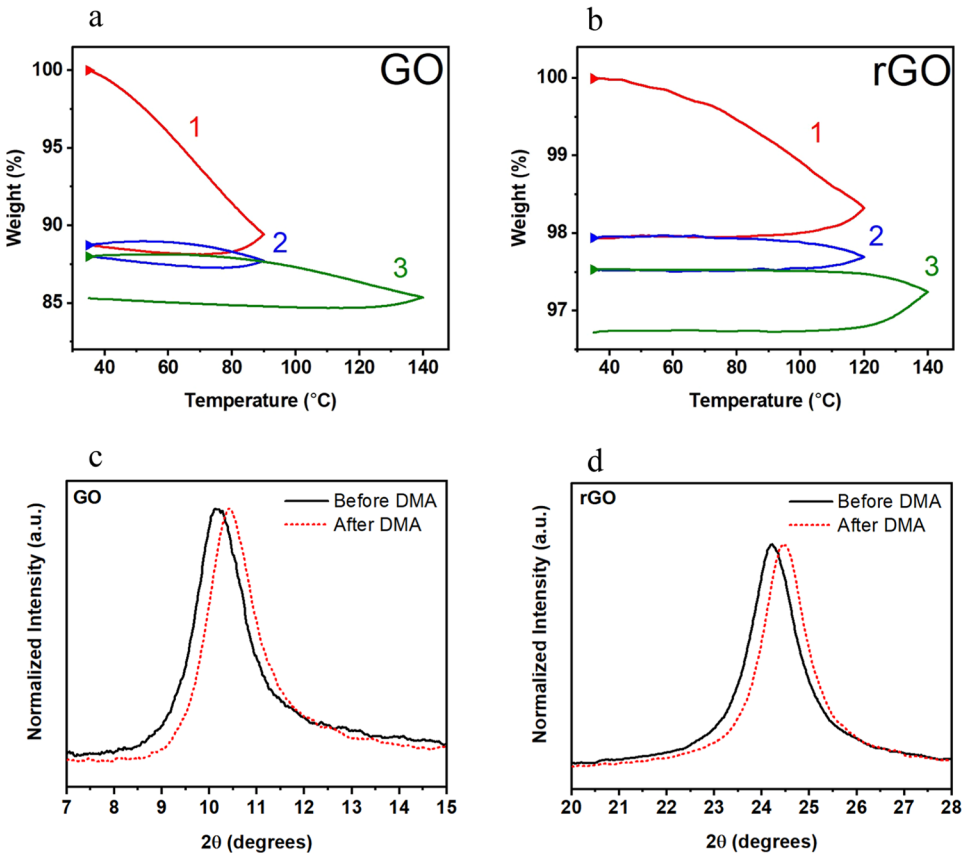


**Figure 4.** TGA curves showing water loss for the (a) GO and (b) rGO samples. XRD patterns of (c) GO and (d) rGO films before and after the DMA testing.

$$\gamma(t) = N_{10} - N_1(t) - \int_0^t \gamma(\tau) N_1(t, \tau) \mathrm{d}\tau \tag{4}$$

Considering the number of active bonds and the rate of reattachment of the broken bonds, one can calculate the total energy of the bulk system as

$$\psi = N_a(t, T)\psi_0(F^{0\to t}) + \int_0^t \gamma(\tau) N_a(t, \tau)\psi_0(F^{\tau\to t})\mathrm{d}\tau - p(J^{0\to t} - 1) \tag{5}$$

where $\psi_0$ is the strain energy of a single bond which is assumed to be a quadratic function of strain in the main direction. These equations are solved numerically for a harmonic force to calculate the storage and loss modules of the GO sheets. The material parameters related to the number of active bonds are estimated through a max−min optimization process to mimic the experimental results.

## 3. RESULTS AND DISCUSSION

SEM images of dispersed GO particles were used to create a histogram of their respective sizes, shown in Figure 2. The mean GO particle size was determined to be 0.85 $\mu$m. Figure 2 micrographs of samples fractured in tension show the layered structure of the GO and rGO films. Both films displayed typical corrugations found in similar films; however, the rGO film was thinner and less corrugated. The cross section of the GO film exhibited more "terraces", while the cross section of rGO showed more "shelves". The presence of "terraces" suggests cracks passing across particle edges and stronger interparticle bonding, while "shelves" indicate cracks propagating between sheets due to weaker interactions.

To evaluate the damping behavior of the GO and rGO films, their viscoelastic response was analyzed using DMA in the tension mode. Figure 3 shows the storage moduli, loss moduli, and tan $\delta$ values of samples at different temperatures. Measured storage moduli values were in the range of 10−20 GPa; an order of magnitude larger than typical polymers and approaching stiffness of quasi-isotropic carbon fiber composites. GO films exhibited a higher modulus compared to rGO ones, which is consistent with the cross-sectional fracture features shown in Figure 2d, indicating stronger interparticle interactions in GO films. Although denser, rGO particles have fewer functional groups, resulting in weaker interparticle interactions.

In sharp contrast to polymers, both GO and rGO samples exhibited a drastic increase in the storage modulus with temperature.[25,31] This phenomenon can be attributed to two mechanisms: the removal of intercalated water and the rearrangement of film layers, resulting in more interactions between the sheets. In GO films, layers packed with highly oxidized particles are bonded to other layers, as well as water. Water intercalated in the films, in a small amount, can facilitate stress transfer across layers,[19] but excess water can act as an inhibitor, blocking two touching layers from effective stress transfer. As water is removed with heat, the available locations for bonding between layers increase, which ultimately leads to material stiffening. In rGO, layers are not highly functionalized, and subsequently, the water between the sheets acts like lubricant, allowing layers to slide past one another easily. This sliding effect is reduced significantly as the water is removed with heat, especially above 70 °C, leading to the observed


https://doi.org/10.1021/acsami.3c15671
ACS Appl. Mater. Interfaces 2024, 16, 11778−11786

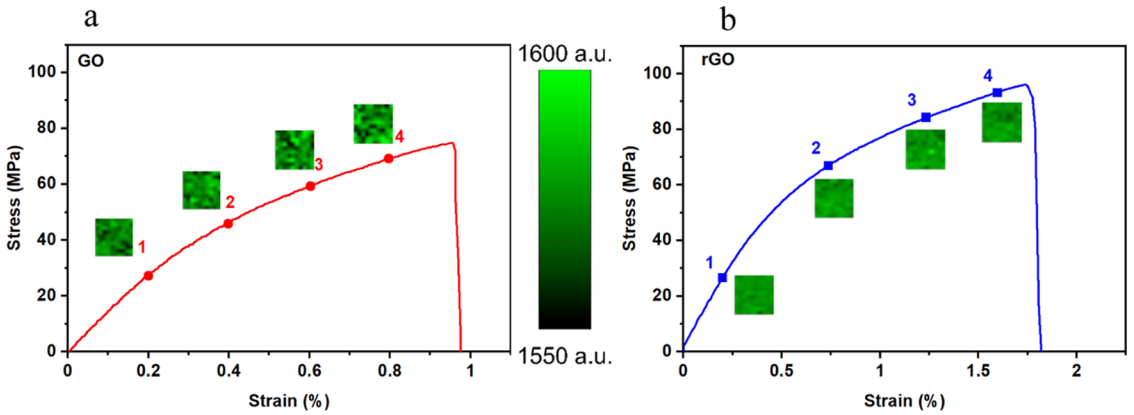


**Figure 5.** In situ tensile Raman mapping of (a) GO and (b) rGO films. A representative strain curve with Raman maps shows the center location of the Raman G-peak at different strains. There are a total of 100 pixels of 15 $\mu$m × 15 $\mu$m in each Raman map.

increase in stiffness. The effect of intercalated water on stiffness (storage modulus) is discussed in more detail later.

The cyclic application of stress can also lead to a change in the stiffness for both films. As stress is continually applied, layers are shuffled to accommodate deformation. This rearrangement can lead to stronger interlayer bonding and more efficient stress transfer, with a consequent increase in stiffness.[15] A similar trend has been observed by other researchers in which the Young's modulus of GO films can increase due to a self-reinforcing behavior through the use of cyclic microbridging.[21] Further exploration of the stiffening phenomena in these films can be found in Figure S3 in the Supporting Information.

The loss modulus was relatively stable with temperature for the GO and rGO samples, less than 20% change over the measured temperature range. Compared to the drastic changes seen in the storage modulus, i.e., 50%, the loss modulus can be considered as temperature-independent for both GO and rGO.

The tan $\delta$ values reached a maximum of near 0.3 for GO and over 0.4 for rGO. To put this in perspective, almost all polymers exhibit a tan $\delta$ of less than 0.1 below their glass transition temperatures. On average, rGO showed higher damping values than GO due to the higher storage modulus of GO. It is apparent that the tan $\delta$ value drops with increasing temperature, which is attributed to the increase in storage modulus.

Structure and water content of tested films before and after the DMA testing (applied stress and heat) were probed by using SEM, TGA, and XRD. Structural features measured via these techniques are linked to their DMA response.

TGA was employed to measure the water loss and absorption in GO and rGO films during cycling heating and cooling. Figure 4a illustrates the weight decrease as the temperature rose and its subsequent increase as the temperature was reduced. The weight fluctuation can be attributed to water loss and subsequent gain. This behavior was observed both below and, notably, above the boiling temperature of water, implying that the lost and absorbed water is intercalated within the GO layers, as previously reported by others.[32] In contrast, nonintercalated water, which is not bound to GO or rGO, would typically evaporate below water's boiling temperature. As this experiment was conducted in air, water was always present in the environment. The water evaporated from previous heating cycles, along with the humidity in the laboratory environment, was partially reabsorbed by the samples upon cooling. As the temperature decreased, GO films regain the ability to retain moisture.[28] It should be noted that the dynamics of water loss and gain do not have time to reach equilibrium at peak temperatures; i.e., intercalated water loss and gain are not instantaneous. This ability to regain water is due to the hydrophilic nature of the highly functionalized GO particles that can bond with atmospheric moisture.

Water loss at elevated temperatures was also evident in the rGO films, as shown in Figure 4b. A much smaller water loss was observed when heating up the rGO film from near-room temperature to the peak temperature of the initial cycle. This could be due to either a lower water content present in the film after reduction and the subsequent ethanol washing process or because any remaining water was trapped in hydrophobic sheets. Unlike GO films, rGO films are hydrophobic and therefore did not absorb water during cooling. Most crucially, the TGA results verified the water loss in GO and rGO films as the temperature rose. This data helps explain the changes to storage modulus with temperature in DMA testing, as discussed earlier.

The heat and stress applied during the DMA tests modified the structure of the films. To quantify these changes, XRD analyses of the films before and after DMA testing were carried out, as shown in Figure 4c,d. Graphitic structures typically have one major $2\theta$ peak, located near 10 or 25°, depending on their oxidation level. Using Bragg's law, the location of the peak can be used to understand the interlayer spacing of GO and rGO particles within tested films. A shift to higher angles indicates a decrease in the interlayer distance. The introduction of oxygen functional groups into GO increases their interlayer spacing. Upon reduction, the peak location for rGO shifts to higher angles, approaching the graphite's $2\theta$ peak location of 26.5°.

There is a noticeable positive peak shift after DMA testing for both samples. The shift is attributed to the paracrystalline regions packing closer to each other due to water loss. This structural change is believed to enhance stress transfer in the films, leading to the increase in stiffness with temperature, as observed in the DMA results presented earlier. This finding aligns with the assumption made in TGA data analysis, suggesting that the water loss and absorption involve molecules intercalated between the GO and rGO particles. Raman spectra of the films were also taken before and after DMA testing to measure any structural changes caused by the heating and stretching in DMA tests; Figure S4. Raman peaks did not


https://doi.org/10.1021/acsami.3c15671
ACS Appl. Mater. Interfaces 2024, 16, 11778−11786

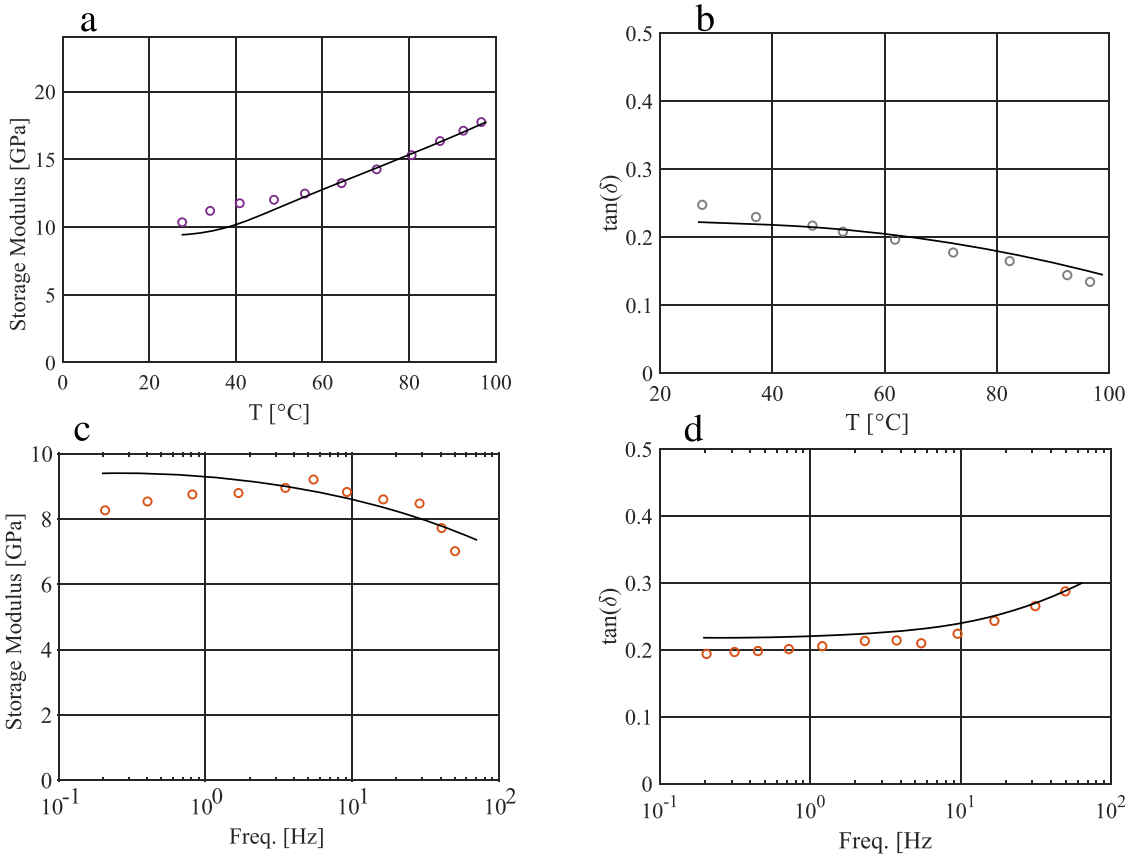


**Figure 6.** Storage modulus and tan $\delta$ of GO film are plotted as a function of temperature (a, b) and frequency (c, d) experimental results (empty circles) in comparison with continuum model prediction (solid lines).

exhibit significant changes between the samples before and after DMA testing.

Results presented so far suggest that water intercalation plays a major role in stress transfer between GO and rGO sheets, affecting their viscoelastic response. To further investigate this, in situ tensile Raman mapping was employed to explicitly show how stress is distributed in GO and rGO films. Film samples were loaded in tension, and Raman maps were captured at several strain levels until failure, providing insights into local stress−strain distributions at each step. Rather than taking a single spectrum, this mapping approach allowed Raman data to be observed over an area of the film. For graphitic materials, two distinct bands, the D band and G band, appear in the 1000−2000 $cm^{-1}$ Raman shift range. The D band represents disorder in the carbon structure and the G band is associated with carbon−carbon bond vibrations in graphitic materials.[33,34] The G-peak shift in Raman spectra of graphene is particularly responsive to the carbon−carbon bond length and overall strain, making it a valuable tool for mapping local deformations. A tensile strain in GO or rGO particles results in a downshift of the G-peak in their spectra.

Figure 5 displays Raman maps of GO and rGO samples acquired from the same location on the films at different global strain values at room temperature. Darker spots in the maps indicate areas under higher tensile strains due to stress transfer, where particles are engaged. Brighter spots signify no stress (slipping and energy release) or compressive stresses. Fluctuations between tension and compression on a micron scale are observed in the Raman maps. It is evident that there are many locations where deformation is not being transferred uniformly, specifically for the GO sample. These spots are due to the voids caused by water pockets of intercalated water, defects stemming from irregular particle arrangements, and microslippage of GO sheets. As mentioned earlier, water can inhibit interparticle interactions. The Raman maps of GO are much more varied than rGO. This aligns with the earlier notion that GO is wavier and contains more water pockets than its reduced counterpart, which is an indicator of the compactness of the films.

Figure 6 compares the model's predictions with experimental results for both temperature and frequency sweeps. The model is based on the nanoscale stick−slip behavior of GO sheets. As the GO layers move relative to each other, the transferred force and the number of broken bonds between the sheets evolve in each cycle, which results in energy dissipation in the system. The continuum model of stochastic debonding can describe the dynamic behavior of the bulk GO films, as evident by the fact that the model predictions align well with the experimental dynamic behavior of the film. Damping occurs when a bond breaks, and it is assumed that the energy stored in the bond is instantaneously released to the environment.

## 4. SUMMARY AND CONCLUSIONS

The unique combination of high stiffness and high damping presented in this study is more pronounced when compared to that of conventional materials. Figure 7 displays an Ashby plot of conventional materials, illustrating the room-temperature loss coefficient (tan $\delta$) against Young's modulus (stiffness). High damping materials are typically soft, making them


https://doi.org/10.1021/acsami.3c15671
ACS Appl. Mater. Interfaces 2024, 16, 11778−11786

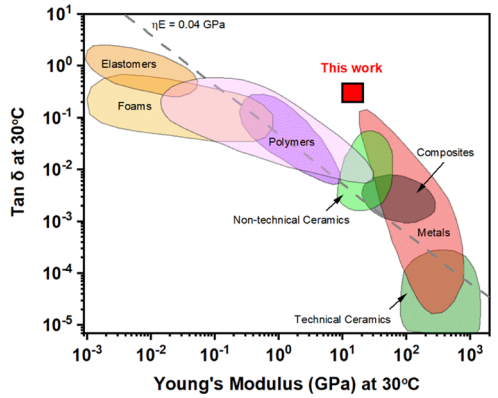


**Figure 7.** Ashby plot comparing the loss coefficient of common dampeners and the materials focused on in this study.

unsuitable for structural situations. As Young's modulus increases, the damping tends to decrease considerably. The films in this study are capable of high damping and high stiffness at room and elevated temperatures, and their density is comparable to polymers and composites. Incorporating GO or rGO films onto the surfaces of structural components offers a smart solution for vibration attenuation with a negligible increase in weight. These performance characteristics render GO and rGO films superior to those of traditional materials used for damping applications.

In this study, the viscoelastic behaviors of GO and rGO films were evaluated using DMA. The findings showed that both films exhibit a high modulus and drastic rises in their storage moduli with increasing temperature. This behavior was attributed to the removal of the intercalated water and structural rearrangement. While less densely packed, GO films possess a higher modulus than rGO films due to their abundant functional groups, resulting in stronger interparticle interactions. The tan $\delta$ values highlighted enhanced damping capabilities in these materials compared to typical polymers. Structural and water content analyses via various characterization techniques affirmed these observations, with the role of hydrogen bond networks in stress transfer and energy dissipation emphasized. The experimental and modeling results suggest that intermittent slippage and hydrogen bonds between the GO and rGO layers contribute significantly to the damping behavior of the films. These bonds act as active energy dissipating mechanisms that break and reform during cyclic loading, leading to the high damping properties observed in the films.

## ■ ASSOCIATED CONTENT

### Supporting Information

The following files are available free of charge. The Supporting Information is available free of charge at https://pubs.acs.org/doi/10.1021/acsami.3c15671.

Additional experimental details, materials, and methods, including FTIR, XPS, Raman spectroscopy, and additional DMA testing (PDF)

## ■ AUTHOR INFORMATION


### Corresponding Author

**Mehran Tehrani** − *Walker Department of Mechanical Engineering, The University of Texas at Austin, Austin, Texas 78712, United States; Department of Structural Engineering, University of California San Diego, La Jolla, California 92093, United States; Program in Materials Science and Engineering, University of California San Diego, La Jolla, California 92093, United States;* Present Address: Mehran Tehrani - Department of Structural Engineering, University of California San Diego, La Jolla, California 92093, United States.; orcid.org/0000-0002-6508-7093; Email: tehrani@ucsd.edu

### Authors

**Gehan C. Jayatilaka** − *Walker Department of Mechanical Engineering, The University of Texas at Austin, Austin, Texas 78712, United States;* Present Address: Gehan Jayatilaka - Walker Department of Mechanical Engineering, The University of Texas at Austin, Austin, Texas 78712, United States

**Athena Aber** − *Department of Structural Engineering, University of California San Diego, La Jolla, California 92093, United States;* Present Address: Athena Aber - Department of Structural Engineering, University of California San Diego, La Jolla, California 92093, United States.

**Moein Mohammadi** − *Walker Department of Mechanical Engineering, The University of Texas at Austin, Austin, Texas 78712, United States;* Present Address: Moein Mohammadi - Walker Department of Mechanical Engineering, The University of Texas at Austin, Austin, Texas 78712, United States.

**Vahid Morovati** − *Department of Civil and Environmental Engineering, University of Connecticut, Storrs, Connecticut 06269, United States; Polymer Program, Institute of Materials Science, University of Connecticut, Storrs, Connecticut 06269, United States;* Present Address: Vahid Morovati - Department of Civil and Environmental Engineering, University of Connecticut, Storrs, Connecticut 06269, United States.

Complete contact information is available at: https://pubs.acs.org/10.1021/acsami.3c15671


### Author Contributions

The manuscript was written through contributions of all authors. All authors have approved the final version of the manuscript.

### Notes

The authors declare no competing financial interest.

## ■ ACKNOWLEDGMENTS

The authors acknowledge the support of the National Science Foundation (NSF) CAREER Award # 2341825.

## ■ REFERENCES


(1) Zhang, J.; Perez, R. J.; Lavernia, E. J. Documentation of Damping Capacity of Metallic, Ceramic and Metal-Matrix Composite Materials. *J. Mater. Sci.* **1993**, *28* (9), 2395−2404.

(2) Lu, H.; Wang, X.; Zhang, T.; Cheng, Z.; Fang, Q. Design, Fabrication, and Properties of High Damping Metal Matrix Composites—a Review. *Materials* **2009**, *2* (3), 958−977, DOI: 10.3390/ma2030958.

(3) Zhang, C. M.; Chen, Y. J.; Li, H.; Liu, H. Z. Facile Fabrication of Polyurethane/Epoxy Ipns Filled Graphene Aerogel with Improved Damping, Thermal and Mechanical Properties. *RSC Adv.* **2018**, *8* (48), 27390−27399, DOI: 10.1039/C8RA04718A.

(4) Soovere, J.; Drake, M. Aerospace Structures Technology Damping Design Guide *Technology Review* 1985; Vol. *1*.

(5) Zeng, X.; Ye, L.; Sun, R.; Xu, J.; Wong, C.-P. Observation of Viscoelasticity in Boron Nitride Nanosheet Aerogel. *Phys. Chem. Chem. Phys.* **2015**, *17* (26), 16709−16714.
(6) Ritchie, I. G.; Pan, Z. L. High-Damping Metals and Alloys. *Metall. Trans. A* **1991**, *22* (3), 607−616.
(7) Chung, D. D. L. Review: Materials for Vibration Damping. *J. Mater. Sci.* **2001**, *36* (24), 5733−5737.
(8) Schaller, R. Metal Matrix Composites, a Smart Choice for High Damping Materials. *J. Alloys Compd.* **2003**, *355* (1), 131−135.
(9) Zhou, X.; Shin, E.; Wang, K. W.; Bakis, C. E. Interfacial Damping Characteristics of Carbon Nanotube-Based Composites. *Compos. Sci. Technol.* **2004**, *64* (15), 2425−2437.
(10) Nieto, A.; Lahiri, D.; Agarwal, A. Synthesis and Properties of Bulk Graphene Nanoplatelets Consolidated by Spark Plasma Sintering. *Carbon* **2012**, *50* (11), 4068−4077.
(11) Chen, B.; Ma, N.; Bai, X.; Zhang, H.; Zhang, Y. Effects of Graphene Oxide on Surface Energy, Mechanical, Damping and Thermal Properties of Ethylene-Propylene-Diene Rubber/Petroleum Resin Blends. *RSC Adv.* **2012**, *2* (11), 4683−4689.
(12) Singh, S.; Rathi, K.; Pal, K. Synthesis, Characterization of Graphene Oxide Wrapped Silicon Carbide for Excellent Mechanical and Damping Performance for Aerospace Application. *J. Alloys Compd.* **2018**, *740*, 436−445.
(13) Li, T.; Du, J.; Xu, M.; Song, Z.; Ren, M. Lightweight and Flexible Graphene Foam Composite with Improved Damping Properties. *Nanomaterials* **2022**, *12* (8), 1260.
(14) Mkhoyan, K. A.; Contryman, A. W.; Silcox, J.; Stewart, D. A.; Eda, G.; Mattevi, C.; Miller, S.; Chhowalla, M. Atomic and Electronic Structure of Graphene-Oxide. *Nano Lett.* **2009**, *9* (3), 1058−1063.
(15) Dikin, D. A.; Stankovich, S.; Zimney, E. J.; Piner, R. D.; Dommett, G. H. B.; Evmenenko, G.; Nguyen, S. T.; Ruoff, R. S. Preparation and Characterization of Graphene Oxide Paper. *Nature* **2007**, *448* (7152), 457−460.
(16) Pei, S.; Zhao, J.; Du, J.; Ren, W.; Cheng, H.-M. Direct Reduction of Graphene Oxide Films into Highly Conductive and Flexible Graphene Films by Hydrohalic Acids. *Carbon* **2010**, *48* (15), 4466−4474.
(17) Cheng, H.; Huang, Y.; Cheng, Q.; Shi, G.; Jiang, L.; Qu, L. Self-Healing Graphene Oxide Based Functional Architectures Triggered by Moisture. *Adv. Funct. Mater.* **2017**, *27* (42), No. 1703096, DOI: 10.1002/adfm.201703096.
(18) Ortiz-Young, D.; Chiu, H.-C.; Kim, S.; Voïtchovsky, K.; Riedo, E. The Interplay between Apparent Viscosity and Wettability in Nanoconfined Water. *Nat. Commun.* **2013**, *4* (1), No. 2482, DOI: 10.1038/ncomms3482.
(19) Medhekar, N. V.; Ramasubramaniam, A.; Ruoff, R. S.; Shenoy, V. B. Hydrogen Bond Networks in Graphene Oxide Composite Paper: Structure and Mechanical Properties. *ACS Nano* **2010**, *4* (4), 2300−2306.
(20) Bobylev, S. V.; Sheinerman, A. G. Effect of Crack Bridging on the Toughening of Ceramic/Graphene Composites. *Rev. Adv. Mater. Sci.* **2018**, *57* (1), 54−62.
(21) Wu, Q.; Su, Y.-j.; Liu, L.-q.; Zhang, Z. Surface Effect on the Self-Reinforcing Behavior of Graphene Oxide Membranes. *Carbon* **2018**, *129*, 403−408.
(22) Wang, L.-F.; Ma, T.-B.; Hu, Y.-Z.; Wang, H. Atomic-Scale Friction in Graphene Oxide: An Interfacial Interaction Perspective from First-Principles Calculations. *Phys. Rev. B* **2012**, *86* (12), No. 125436.
(23) Shen, X.; Lin, X.; Yousefi, N.; Jia, J.; Kim, J.-K. Wrinkling in Graphene Sheets and Graphene Oxide Papers. *Carbon* **2014**, *66*, 84−92.
(24) Pei, S.; Cheng, H.-M. The Reduction of Graphene Oxide. *Carbon* **2012**, *50* (9), 3210−3228.
(25) Hu, K.; Cardenas, W.; Huang, Y.-C.; Wei, H.; Gaskell, R.-E.; Martel, E.; Cerruti, M.; Szkopek, T. Viscoelastic Response of Graphene Oxide-Based Membranes and Efficient Broadband Sound Transduction. *Adv. Funct. Mater.* **2022**, *32* (8), No. 2107167, DOI: 10.1002/adfm.202107167.
(26) Li, T.; Meng, Z.; Keten, S. Interfacial Mechanics and Viscoelastic Properties of Patchy Graphene Oxide Reinforced Nanocomposites. *Carbon* **2020**, *158*, 303−313.
(27) Su, Y.; Wei, H.; Gao, R.; Yang, Z.; Zhang, J.; Zhong, Z.; Zhang, Y. Exceptional Negative Thermal Expansion and Viscoelastic Properties of Graphene Oxide Paper. *Carbon* **2012**, *50* (8), 2804−2809.
(28) Patra, S.; Veettil, V. T.; Narayanan, T. N. Enhanced Viscoelastic Properties of Graphene Oxide Membranes. *Carbon* **2017**, *124*, 576−583.
(29) Qin, Z.; Buehler, M. J. Cooperative Deformation of Hydrogen Bonds in Beta-Strands and Beta-Sheet Nanocrystals. *Phys. Rev. E* **2010**, *82* (6), No. 061906.
(30) Long, R. Time Dependent Behavior of a Dual Cross-Link Self-Healing Gel: Theory and Experiments. *Macromolecules* **2014**, *v 47* (no. 20), 7243−7250, DOI: 10.1021/ma501290h. −2014 v.47 no.20.
(31) An, Z.; Compton, O. C.; Putz, K. W.; Brinson, L. C.; Nguyen, S. T. Bio-Inspired Borate Cross-Linking in Ultra-Stiff Graphene Oxide Thin Films. *Adv. Mater.* **2011**, *23* (33), 3842−3846.
(32) Farivar, F.; Yap, P. L.; Karunagaran, R. U.; Losic, D. Thermogravimetric Analysis (Tga) of Graphene Materials: Effect of Particle Size of Graphene, Graphene Oxide and Graphite on Thermal Parameters. *C* **2021**, *7* (2), No. 41, DOI: 10.3390/c7020041.
(33) Bîru, E. I.; Iovu, H. Graphene Nanocomposites Studied by Raman Spectroscopy. In *Raman Spectroscopy*; InTech, 2018.
(34) Kudin, K. N.; Ozbas, B.; Schniepp, H. C.; Prud'homme, R. K.; Aksay, I. A.; Car, R. Raman Spectra of Graphite Oxide and Functionalized Graphene Sheets. *Nano Lett.* **2008**, *8* (1), 36−41.